In the second stage, these clusters arrange themselves to form the tetragonal long-range order, as seen in the small regions, *a*, *b* and *c*, in Fig. 7. The fact that such tetragonal regions always take trigonal orientations supports the above conclusion that the polyatomic Bi–Mn clusters in the first stage have twelvefold symmetry. In comparing the square unit patterns in Fig. 4 (more clearly in Fig. 7) with the doughnut-shaped contrasts in Fig. 5, it seems that a little deformation will be necessary for the clusters to build up the tetragonal lattice in the second stage, in order to satisfy the lowering of symmetry from twelve- to fourfold, as was also suggested by Audier & Guyot (1988).

References

AUDIER, M. & GUYOT, P. (1988). *Proc. 5th Jpn Inst. Met. Int. Symp. (JIMIS-5) Non-Equilibrium Solid Phases Met. Alloys*, Kyoto, 1988, p. 467.

CHEN, D. (1971). *J. Appl. Phys.* **42**, 3625–3628.

HONDA, S. & KUSUDA, T. (1974). *J. Appl. Phys.* **45**, 2689–2692.

IWAMA, Y., MIZUTANI, U. & HUMPHREY, F. B. (1972). *IEEE Trans. Magn.* **8**, 487–489.

UNGER, Y. & STOLZ, M. (1971). *J. Appl. Phys.* **42**, 1085–1089.

WILLIAMS, H. J., SHERWOOD, R. C., FOSTER, F. G. & KELLEY, E. M. (1957). *J. Appl. Phys.* **28**, 1181–1184.

YOSHIDA, K., YAMADA, T. & FURUKAWA, Y. (1986). *Acta Metall.* **34**, 969–979.

YOSHIDA, K., YAMADA, T. & TANIGUCHI, Y. (1987). *14th Int. Congr. Crystallogr.*, Perth, 1987. Collected Abstracts, p. C-123.

Acta Cryst. (1989). B**45**, 45–52

Electron Density, Thermal Motion and Bonding Interactions in the Perovskite Structures KMF_3 with M = Mn, Fe, Co and Ni

BY E. N. MASLEN AND N. SPADACCINI

Crystallography Centre, University of Western Australia, Nedlands 6009, *Australia*

(*Received* 17 *July* 1988; *accepted* 20 *September* 1988)

Abstract

The KMF_3 structures with M = Mn, Fe, Co and Ni have been investigated in detail using data from previous studies. The vibration amplitudes, atomic charges determined by difference density partitioning and the heights of characteristic features of the difference densities change monotonically through the series. Trends in the difference densities are consistent with the expected variation of the exchange contribution (antisymmetrization of the electron wavefunction) with the occupancy of the 3*d* subshell. The redistribution of electron density in the region of overlap of the atomic orbitals for the transition-metal and F atoms reflects mainly the effects of that exchange. The topography also shows the consequences of interactions between the transition-metal and the next-nearest-neighbour K atoms. There are local maxima or minima in the difference densities further from the nuclei. The sign of the difference density at these regions of low electrostatic potential depends on the chemical identity of the M species.

Introduction

Information contained in difference electron densities from X-ray diffraction experiments extends our understanding of chemical bonding. The detailed three-dimensional image of the electron density from an accurate diffraction experiment provides a benchmark against which the validity of models for chemical bonding can be tested. At a qualitative level the predictions of the model can be checked for consistency with the topography of the electron density. The ultimate objective is to predict properties as completely as possible from the one electron density function.

The simplest case is that of a series of isomorphous compounds in which only one type of atom varies. The environment remains approximately constant if the electronic structure of just one atom changes. The Mn, Fe, Co and Ni members of the KMF_3 series crystallize in the cubic space group $Pm3m$ and with the ideal perovskite structure (Wyckoff, 1964). The atoms are located at the special positions M(0,0,0), K($\frac{1}{2},\frac{1}{2},\frac{1}{2}$) and F($\frac{1}{2}$,0,0) and have low temperature factors. The transition metal is coordinated to six F atoms in an ideal octahedron. The second-nearest neighbours consist of eight K atoms located in the $\langle 111 \rangle$ directions of that octahedron. Difference densities for these compounds have been described earlier (Kijima, Tanaka & Marumo, 1981, 1983; Miyata, Tanaka & Marumo, 1983). Those studies accurately displayed the rearrangement of the transition-metal *d* electrons as a result of the crystal field and determined relative populations for the t_{2g} and e_g orbitals. The magnitude of the redistribution of electron density increases progressively through the series, in line with the increase in the polarizability expected for the transition metal.

0108-7681/89/010045-08$03.00

There is some ambiguity in terminology resulting from indiscriminate use of terms such as binding, bonding, antibonding, attractive and repulsive. Binding and bonding are often used interchangeably, but some authors carefully distinguish the subtle difference between them. Binding relates to the forces acting on the *nuclei* (Berlin, 1951) in molecule formation while bonding relates to changes in energy (Spackman & Maslen, 1985). In the simple case of a diatomic promolecule, a model consisting of spherically symmetric overlapping but undeformed charge-density clouds, there is a deep minimum in the energy curve, that is to say it is bonding, but the forces repel the nuclei for all separations, that is, it is unbound. However binding can be achieved by a very small displacement of the nuclei relative to their atomic electron clouds. Chemical properties are dominated by the terms relating to the energy (bonding). The additional term with sharp energy gradients required for binding may be treated as small perturbations. Throughout this paper *bonding* energy is preferred to the more common term *binding* energy. Its negative sign is retained so that the most stable state has the minimum bonding energy. Bonding and antibonding here refer to the sign of that energy contribution, negative in the former case and positive in the latter.

Refinement

The data from the earlier studies, obtained from material deposited with the British Library Document Supply Centre as Supplementary Publications, are of good quality, with each reflection profile scanned up to ten times to reduce statistical and other errors. The data were corrected for absorption and type I anisotropic extinction.

The original refinements were based on models incorportating ionic structure factors some of which were spherically averaged, while others were derived from atoms in differing spin states.

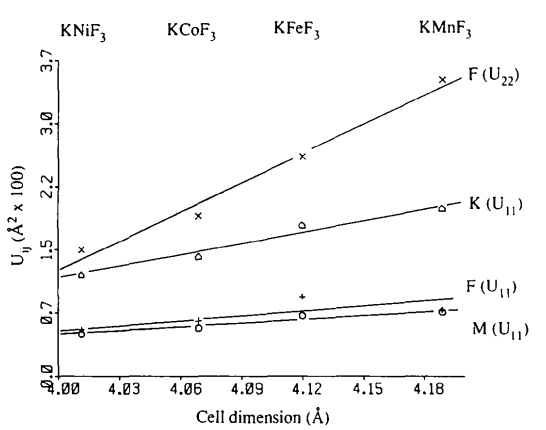

Fig. 1. Thermal vibration amplitudes for the KMF_3 compounds as a function of cell dimension.

The structures were reanalyzed using a set of harmonically vibrating free atoms as the reference model, minimizing $\sum(|F_r| - k|F_c|)^2$. The scattering factors were those of Cromer & Mann (1968). Anomalous-dispersion corrections were taken from Cromer & Liberman (1970). For $KMnF_3$ and $KNiF_3$, extinction was included in the refinement, following the method of Larson (1970) in which only the isotropic component of secondary extinction is considered. Structural parameters are minimally affected by the difference between ionic and atomic scattering factors (Spackman, Hill & Gibbs, 1987) and refinements with position and thermal parameters fixed at those values reported by the original authors were satisfactory. All calculations were carried out with the *XTAL* system of crystallographic programs (Hall & Stewart, 1988).

The difference densities for the new refinements closely resembled those published originally, indicating that bias in the structural parameters caused by the choice of reference model was minimal. The close agreement between the structure factors of equivalent reflections for $KMnF_3$ and $KNiF_3$ was indicated by the low values of the merging R_{int} factor (0·009 and 0·008 respectively). Confining the extinction correction to the isotropic model resulted in R factors and difference densities virtually identical to those reported by the original authors. Any anisotropy in the extinction must be small *i.e.* the extinction is essentially isotropic for this series of structure analyses. If isotropic extinction is also preferred to the anisotropic model for the related $KCuF_3$ member of the series, the difference densities are more consistent with the rest of the series (Spadaccini & Maslen, 1987).

The MF_6 chromophore is an ideal octahedron with M—F bond lengths ranging from 2·0058 to 2·0945 Å. The second coordination sphere consists of eight K atoms in the ⟨111⟩ directions, pointing at the faces of the octahedron, at distances from 3·4741 to 3·6277 Å. Because of the high atomic site symmetries in these structures, the bond and contact distances through the series are exact linear functions of the cell dimension. Other chemical or physical properties which are correlated to interatomic separation will thus display correlation with cell dimension. The M and K thermal parameters are isotropic, by site symmetry, with B values ranging from 0·388 to 0·595 Å^2 and from 0·945 to 1·570 Å^2 respectively. The atomic thermal parameters are plotted against cell dimension in Fig. 1. With the exception of the U_{11} term for the F atom in $KMnF_3$ the variation is close to linear. The magnitudes are lowest for the Ni structure. The effective radius of the transition metal decreases from Mn to Ni owing to the increased effective nuclear charge which is reflected in the reduction in cell size. The decreasing magnitudes of the thermal parameters show that the reduced radius of the transition-metal atom from the Mn structure to the Ni structure, indicated in Fig. 1, results in tighter

Table 1. *Net atomic charges* (e) *from the Hirshfeld partitioning of* $\Delta\rho$

	Formal	$KMnF_3$	$KFeF_3$	$KCoF_3$	$KNiF_3$
M	2	0·09	0·20	0·39	0·41
K	1	0·24	0·32	0·32	0·46
F	−1	−0·11	−0·18	−0·24	−0·29
MF_6	−4	−0·57	−0·85	−1·03	−1·33

packing, restricting the freedom of movement of the atoms in the structure as a whole.

Atomic charges

The electron transfer in ionic solids is often described in terms of the formal values idealized as point charges at the nuclei. The large charge transfers associated with formal values in the ionic model exaggerate the real movement of electron density (Slater, 1965). Development of physically realistic models requires more accurate assessment of the charge on an atom in the solid.

The method of partitioning of Hirshfield (1977) yields consistent and chemically reasonable results (Maslen & Spackman, 1985). The magnitudes of the charges determined for mononuclear ions in a large number of systems are much less than the formal values. Studies of transition-metal Tutton salts and sulfate pentahydrates by the Hirshfeld method give consistent results both for mononuclear and charged groups. Charges for the sulfate groups are −1·22 e in the Cu Tutton salt (Maslen, Watson & Moore, 1988), −1·01 e for the Zn salt (Maslen, Watson, Ridout & Moore, 1988), −1·10 and −1·08 e in the Mg and Ni salts (Maslen, Ridout & Watson, 1988). The sulfate charges for Cr and Cu sulfate pentahydrate are −0·97 and −1·20 e respectively (Vaalsta & Maslen, 1987).

The atomic charges determined for the potassium transition-metal trifluorides by the Hirshfeld method, given in Table 1, are consistent with those of other workers (Bats & Fuess, 1986; Maslen & Spackman, 1985), for a wide range of compounds.

The charges are a small fraction of their formal values, although the atomic species become increasingly ionic in progressing through the series. The variation of the charge with cell dimension, plotted in Fig. 2, is close to linear. The charges for Co and K for the Co structure deviate appreciably from the trend lines for the series as a whole.

Difference densities

The difference densities for these compounds should reflect the change in electronic configuration of the transition metal as one progresses along the row from Mn to Ni. The lattice environment is identical, except for the small variations in cell dimensions and contact distances.

The difference densities in the plane perpendicular to the fourfold axis containing four *M*—F bonds for the four compounds are shown in Fig. 3. We focus initially on the features near the transition-metal nuclei. The difference density along the *M*—F bond shows effects commonly associated with overlap of the atomic orbitals. For Mn there is a peak, approximately 0·6 Å from the metal nucleus, 0·5 e Å^{-3} in height, directed toward the F atom. In the Fe compound there is a feature with similar radial dependence, but with the peak replaced by a minimum of −0·3 e Å^{-3}. This trend continues through the series, the feature having a depth of −1·12 e Å^{-3} for $KNiF_3$. This is consistent with what is expected for an exchange term. As the contribution from the antibonding orbitals increases the electrons are repelled more strongly from the vicinity of the *M*—F bond. The depletion increases progressively, becoming more strongly antibonding from Mn to Ni, as the spin conflict resulting from overlap of the F atom's electrons with the 3*d* subshell increases. This is consistent with what is expected from the exclusion principle.

The topology of the difference density in Fig. 3 has a contrasting parallel in Fig. 4, which shows the difference density along the *M*—K interaction vector as well as the *M*—F interaction vector. *M*—K interactions are often regarded as weak, and contributing negligibly to the deformation density near the transition metal. However if we consider the atomic radii of the *M* and K atoms to be half the bond distances found for the elemental solids, the *M*—K contact distances in these compounds are close to the sum of these radii. For neutral atoms such interactions would be significant. In Fig. 4(*a*) there is a minor build up of density (less than one contour) along the Mn—K direction. Whereas the density along the *M*—F vectors becomes more negative this feature becomes increasingly more positive as one progresses through the Fe, Co and Ni analogues, for which it maximizes at 1·13 e Å^{-3}. The peaks are aligned with their maxima along the *M*—K vectors.

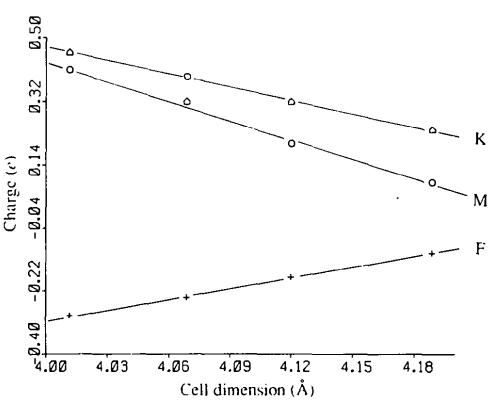

Fig. 2. Atomic charges (e) from the Hirshfeld partitioning of $\Delta\rho$ as a function of cell dimension.

The build up of density along this direction could also be due to the overlap of the M atom with the diffuse orbitals of the K atom. Such a build up would be consistent with an exchange term which is positive *i.e.* lowers the energy. The probable significance of second-nearest-neighbour interactions has also been reported earlier for other compounds (Maslen, Spadaccini & Watson, 1983; Maslen, Spadaccini, Watson & White, 1986; Maslen & Spadaccini, 1987). The difference densities along the M–K vectors in Fig. 4 are comparable with those along cation–cation vectors in those structures.

The variation of characteristics of the difference density with cell dimension through the series is shown in Fig. 5, which depicts the heights at the F atom, in the e_g orbital and in the t_{2g} orbital, projected onto the plane of Fig. 3. The variation is close to linear in all cases. This is not surprising for the densities near atomic sites, since the degree of overlap between the metal atom and the F ligand will obviously change in a regular manner with cell size.

This variation in the heights of characteristic features in the difference density, as one progresses through the series strongly resembles that of the thermal parameters and the atomic charges shown in Figs. 1 and 2. As the effective size of the transition metal decreases from Mn to Ni, the reduced contact distance increases the degree of overlap between the transition metal and the F

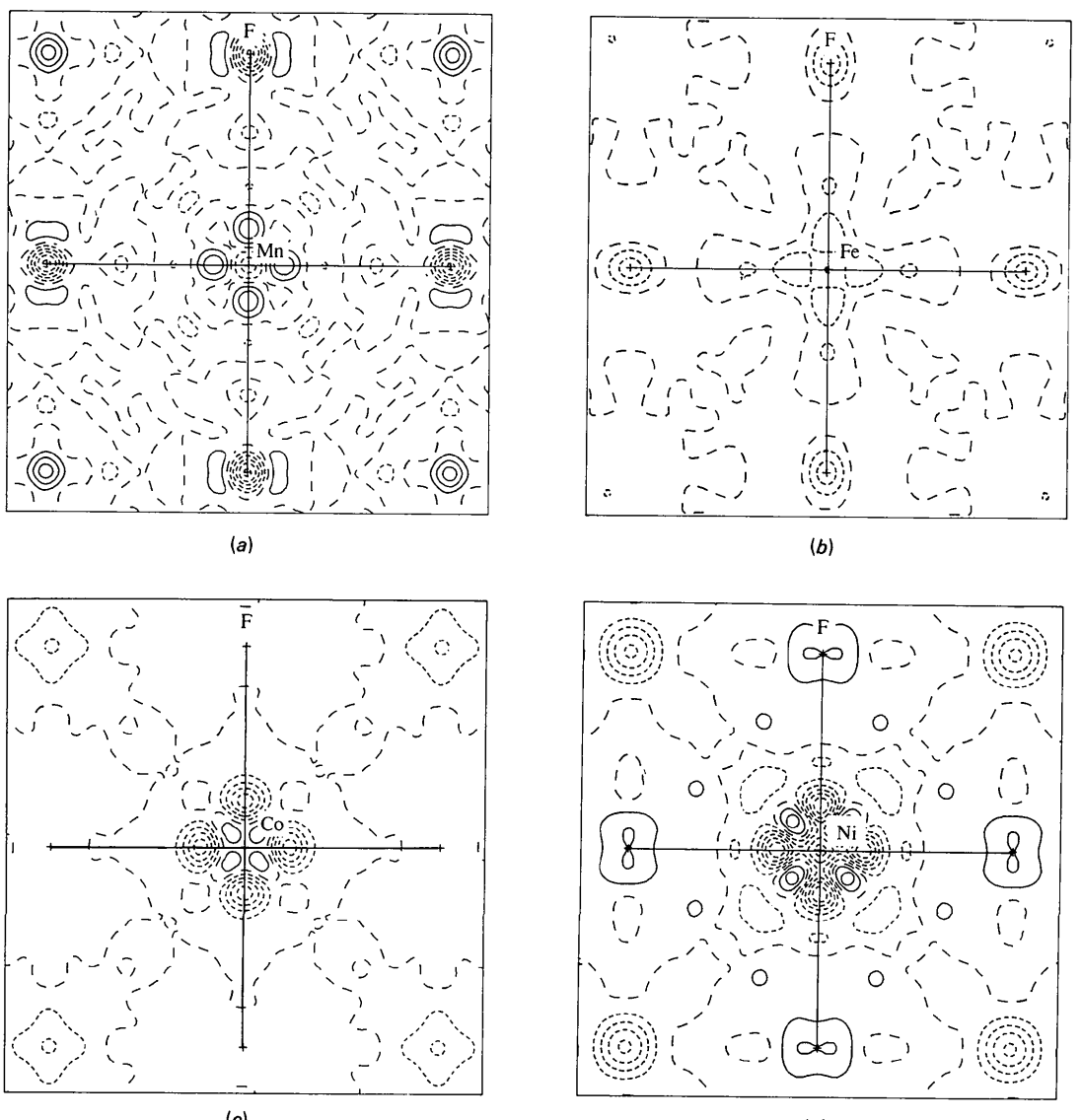

Fig. 3. $\Delta\rho$ in a section through the M–F bonds: (*a*) $KMnF_3$, (*b*) $KFeF_3$, (*c*) $KCoF_3$, (*d*) $KNiF_3$. The contour interval is 0·2 e Å^{-3}. Positive, zero and negative contours – solid, long and short dashes, respectively. Map borders are 5 × 5 Å.

valence orbitals. This compounds the effect of increasing number of d electrons, with the exchange term becoming increasingly antibonding. The difference density near the transition metal is increasingly polarized as one progresses along the series towards Ni, as shown in Fig. 5. The linear variation of the difference densities with cell dimensions is again consistent with what is expected for an exchange term. The movement of density associated with this polarization increases the atomic charges. The lowering of the thermal parameters and the increased density polarization are clearly related. Both result from the compression of the contact distances as the overlap between valence orbitals increases.

The relationship between the packing of atoms, the thermal motion and the polarization of density has been discussed by Henderson & Maslen (1987) for the alkali halides. The electron density is depleted along the cation–cation vectors which are markedly shorter than the corresponding distance in the pure metal, and those cations carry significant positive charges.

This behaviour is also consistent with the well known increase in electronegativity with row number in the Periodic Table. The atoms are increasingly electropositive on progressing down each column. Other things being equal the larger atoms overlap more strongly with their neighbours, and lose electrons as a result of exchange. The closer packing for the KMF_3 series as the cell volume decreases and the atomic number of M increases, indicated by the thermal-motion data, mimics this effect and generates the expected increase in cation charge.

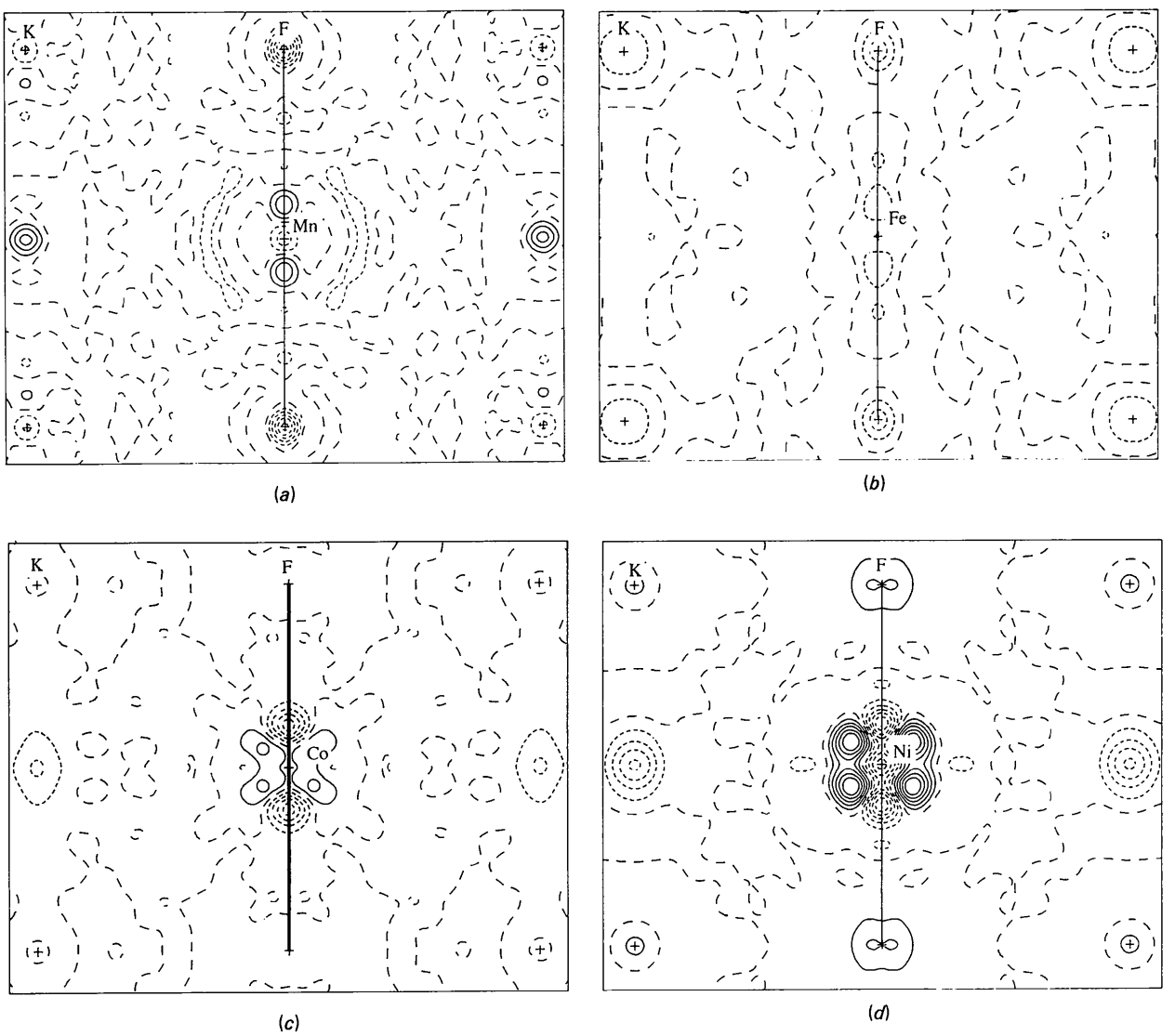

Fig. 4. $\Delta\rho$ in a section through the M–F bonds and including the M–K interaction: (*a*) $KMnF_3$, (*b*) $KFeF_3$, (*c*) $KCoF_3$, (*d*) $KNiF_3$. Contours as in Fig. 3. Map borders are 6·4 × 5 Å.

The effect of increasing the d-subshell population for the M species on the orbital overlap can be understood qualitatively in terms of the changes in the electrostatic energy (E_{es}). This is the classical interaction energy for overlapping, undeformed, spherically symmetric charge-density clouds. Although it is only one term in the expression for the total bonding energy, it can be considered as the first-order term in a perturbation expansion of that energy and is often dominant. The variation of E_{es} with distance for the diatomic interactions in these crystal structures is plotted in Fig. 6.

The strengths of the interactions indicated by the E_{es} values are consistent with the thermal motion data in Fig. 1. The M atoms are involved in six strong M–F and eight M–K interactions, have the lowest electrostatic energies, and the lowest vibration amplitudes. The thermal parameter for the K atom, involved in eight M–K interactions, is about twice as large. The motion of the F atom is strongly anisotropic. In the direction of the M–F bond the amplitudes for the M and F vibrations are comparable, as expected because of the strength of this bond. In the direction of the K–F interaction the F atom is less constrained, and its thermal motion is larger than that of the K atom. Note that E_{es} for K–F is nearer zero than the values for the M–F and M–K interactions. Both the electrostatic energies and the thermal motion indicate that crystal packing does not depend strongly on the K–F interaction. The M–K interaction is more significant.

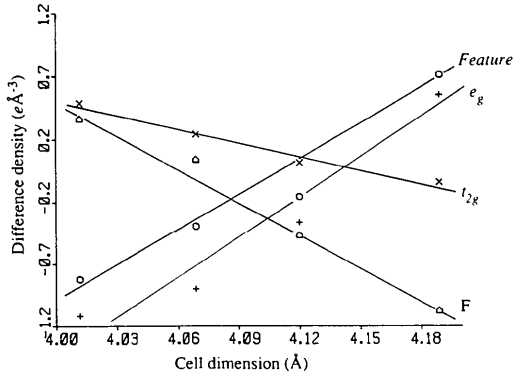

Fig. 5. The magnitudes of $\Delta\rho$ at various points in the cell as a function of cell dimension.

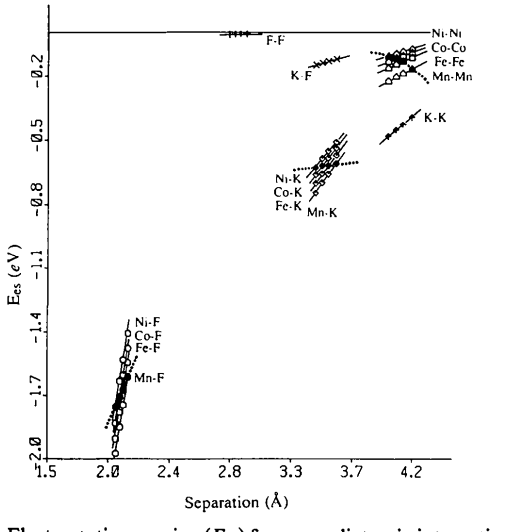

Fig. 6. Electrostatic energies (E_{es}) for some diatomic interactions at various separations. The solid points indicate the contact distances found in the structure.

Table 2. *Electrostatic energies for some interactions in* KMF_3

	$KMnF_3$	$KFeF_3$	$KCoF_3$	$KNiF_3$
M–M	−0·163	−0·127	−0·114	−0·105
K–K	−0·392	−0·426	−0·452	−0·482
F–F	−0·004	−0·005	−0·006	−0·008
M–K	−0·606	−0·616	−0·617	−0·625
M–F	−1·615	−1·677	−1·710	−1·756
K–F	−0·117	−0·127	−0·135	−0·144

E_{es} decreases uniformly with separation but there are marked differences in the energy gradients, indicated by the slopes of the solid lines in Fig. 6. For the interactions involving the transition-metal atoms the shaded points indicate the E_{es} values at the contact distance in the structure as listed in Table 2. The variation of the shaded points (dotted lines) shows the combined effect on the electrostatic interaction energy of decreasing the contact distance and increasing the d-subshell population. Changing the d-shell population has two competing effects on the M–M energy. Raising the number of d electrons increases the degree of overlap, but at a fixed separation this is outweighed by the contraction of the electron cloud due to the increased nuclear charge. The combined effect is to reduce the magnitude of the bonding – to raise the bonding energy.

In addition to the electrostatic interaction energy, the total bonding energy includes contributions from the electron density rearrangement associated with exchange and other polarization terms. The sign of this contribution can be inferred from the difference density topology in the interatomic region.

Consider the M–M interactions. As the contact distance is compressed the bonding E_{es} term becomes more negative. However, a substantial antibonding component arising from the increased d-subshell population must be included, resulting in the dotted curve with the negative slope in Fig. 6. It is less bonding for the Ni–Ni interaction than it is for the Mn–Mn interaction. To this must be added terms associated with the polarization of the electron density, which can be qualitatively inferred in some cases from Fig. 3. This is complicated by the colinearity of the M–F and

M–M vectors, which makes it more difficult to distinguish the two interactions. As shown in Fig. 3(*d*) there is a large deficiency of electrons near the Ni atom, along the Ni–Ni (and Ni–F) vectors. This makes an antibonding contribution to the total bonding energy, which must be more positive than E_{es}. Conversely near the Mn atom there is electron excess along the Mn–Mn (and Mn–F) vector. In this case the contribution is bonding, lowering the total bonding energy below E_{es}. We conclude that the contribution of the polarization to the M–M interactions is increasingly antibonding from $KMnF_3$ to $KNiF_3$.

The same reasoning applies to the M–F interaction, but the combined effect of cell compression and increased *d*-subshell population is electrostatically favourable, $E_{es}(\text{Ni–F}) < E_{es}(\text{Mn–F})$ in this case, as shown by the strong positive slope of the dotted M–F line in Fig. 6. The change in terms associated with the deformation of the charge-density clouds is in the opposite direction.

The M–K interactions are often neglected because of their supposedly small contribution to bonding. Fig. 6 shows that these terms are about one third as strong as the M–F interactions, but the combined contribution of cell compression and increased electron population on the M–K interaction energy is slightly bonding. This is indicated by the weak positive slope of the dotted M–K line. The sign of the contribution of the exchange to the bonding energy is opposite to that for the M–M and M–F interactions, because of the increase in density along the M–K vector as M progresses towards Ni. In $KNiF_3$ there is a large excess of density directly along the Ni–K vector which makes a bonding contribution. The weak depletion of density along the Mn–K vector in $KMnF_3$ will make a slightly antibonding contribution to that interaction energy. The total contribution of the M–K interaction to the bonding energy is increasingly bonding from $KMnF_3$ to $KNiF_3$.

There is a significant feature in the difference density midway between the K atoms in all sections of Fig. 3. In the Mn structure this is a peak of 0·6 e Å^{-3}. It decreases progressively through the series, forming a hollow of −0·8 e Å^{-3} in the Ni structure. A similar result was obtained in a study of the isomorphous $KZnF_3$ compound (Buttner & Maslen, 1988). The difference density in a second study of $KCoF_3$ (Buttner, 1988) using a very small extinction-free crystal has the same topology. Charges derived from the data were less accurate because of the weakness of reflections from the small crystal, but within the accuracy of the experiment agree with the values in Table 1.

This feature is rather isolated, being approximately 2·8 Å from the metal atoms and 2 Å from the K and the F atoms. Although too far from the atomic centres to be attributed to well known chemical effects the variation of the difference density at this site, plotted against cell dimension in Fig. 5 (marked *Feature*), shows the same linear variation as those for other characteristic features in the difference density.

The feature becomes more prominent and more localized with increasing data resolution. The rate of increase is slow, as expected for valence-electron terms. It cannot result from random error and is highly unlikely to arise from similar systematic errors in six different experiments, especially as a careful examination of the data showed no evidence for such error. Difference densities are minimally affected by series termination, and these for the KMF_3 do not have the characteristic shapes of series-termination artefacts. The consequences of ambiguity in the phases of small F_{cal} reflections were investigated but were not consistent with the results observed.

Thus there exists a structural cavity between the F and K atoms which may be a local maximum or minimum in the difference density depending on the chemical species at the M site. The linear variation with cell dimension is similar to that for other features of known origin. This suggests that they arise in the same way.

Enhancement of electron density at a site of low electrostatic potential far from the nuclei could have important consequences in a related series, namely the high T_c $YBa_2Cu_3O_7$ superconductors. The structural geometry of that series is an orthorhombic distortion of the cubic KMF_3 perovskite structure, in which oxygen replaces fluorine, with yttrium and barium replacing potassium in the ratio 1:2. The structural distortion requires a tripling of the perovskite cell in one direction. Two of the oxygen sites in the ideal structure are vacant, the cell having seven O atoms instead of the ideal nine. One of the structural cavities in the ideal cubic structure extends into a channel through the distorted cell. Concentration of valence electron density in that linear region of low electrostatic potential may facilitate electron transport in these superconductors. Further investigation of the electron density in the high T_c superconductors is required to test this hypothesis.

This work was supported by the Australian Research Grants Scheme.

References

BATS, J. W. & FUESS, H. (1986). *Acta Cryst.* B**42**, 26–32.

BERLIN, T. (1951). *J. Chem. Phys.* **19**, 208–213.

BUTTNER, R. H. (1988). Private communication.

BUTTNER, R. H. & MASLEN, E. N. (1988). *Acta Cryst.* C**44**, 1707–1709.

CROMER, D. T. & LIBERMAN, D. (1970). *J. Chem. Phys.* **53**, 1891–1898.

CROMER, D. T. & MANN, J. B. (1968). *Acta Cryst.* A**24**, 321–324.

HALL, S. R. & STEWART, J. M. (1988). Editors. *XTAL*2.4 *User's Manual.* Univs. of Western Australia, Australia, and Maryland, USA.

HENDERSON, J. A. & MASLEN, E. N. (1987). *Acta Cryst.* A**43**, C-102.

HIRSHFELD, F. L. (1977). *Theor. Chim. Acta*, **44**, 129–138.
KIJIMA, N., TANAKA, K. & MARUMO, F. (1981). *Acta Cryst.* B**37**, 545–548.
KIJIMA, N., TANAKA, K. & MARUMO, F. (1983). *Acta Cryst.* B**39**, 557–561.
LARSON, A. C. (1970). In *Crystallographic Computing*, edited by F. R. AHMED. Copenhagen: Munksgaard.
MASLEN, E. N., RIDOUT, S. C. & WATSON, K. J. (1988). *Acta Cryst.* B**44**, 96–101.
MASLEN, E. N. & SPACKMAN, M. A. (1985). *Aust. J. Phys.* **38**, 273–287.
MASLEN, E. N. & SPADACCINI, N. (1987). *Acta Cryst.* B**43**, 461–465.
MASLEN, E. N., SPADACCINI, N. & WATSON, K. J. (1983). *Proc. Indian Acad. Sci.* **92**, 443–448.
MASLEN, E. N., SPADACCINI, N., WATSON, K. J. & WHITE, A. H. (1986). *Acta Cryst.* B**42**, 430–436.
MASLEN, E. N., WATSON, K. J. & MOORE, F. H. (1988). *Acta Cryst.* B**44**, 102–107.
MASLEN, E. N., WATSON, K. J., RIDOUT, S. C. & MOORE, F. H. (1988). *Acta Cryst.* C**44**, 1510–1544.
MIYATA, N., TANAKA, K. & MARUMO, F. (1983). *Acta Cryst.* B**39**, 561–564.
SLATER, J. C. (1965). *Quantum Theory of Molecules and Solids*, Vol. 2. New York: McGraw-Hill.
SPACKMAN, M. A., HILL, R. J. & GIBBS, G. V. (1987). *Phys. Chem. Miner.* **14**, 139–150.
SPACKMAN, M. A. & MASLEN, E. N. (1985). *Acta Cryst.* A**41**, 347–353.
SPADACCINI, N. & MASLEN, E. N. (1987). *Acta Cryst.* A**43**, C-104.
VAALSTA, T. P. & MASLEN, E. N. (1987). *Acta Cryst.* B**43**, 448–454.
WYCKOFF, R. W. G. (1964). *Crystal Structures*, Vol. 2. New York: Wiley.

Acta Cryst. (1989). B**45**, 52–60

Anharmonic Thermal Motion and Low-Temperature Phase Transition in Tetraethylammonium Octahydrido(triphenylphosphine)rhenate(1–)

BY S. C. ABRAHAMS AND P. MARSH

AT&T Bell Laboratories, Murray Hill, New Jersey 07974, *USA*

(*Received* 17 *June* 1988; *accepted* 29 *September* 1988)

Abstract

$[N(C_2H_5)_4][ReH_8\{P(C_6H_5)_3\}]$, $M_r = 586{\cdot}81$, orthorhombic with lattice constants at 295 K of $a = 10{\cdot}615\ (3)$, $b = 25{\cdot}338\ (7)$ and $c = 10{\cdot}134\ (2)$ Å, $V = 2725{\cdot}6\ (1{\cdot}2)$ Å^3 in space group $P2_12_12_1$ with $Z = 4$; at 163 K, monoclinic with $a = 10{\cdot}497\ (3)$, $b = 24{\cdot}970\ (10)$, $c = 10{\cdot}067\ (4)$ Å and $\beta = 91{\cdot}06\ (3)°$, $V = 2638{\cdot}2\ (1{\cdot}7)$ Å^3 in space group $P2_1$ with $Z = 4$. $F(000) = 1184$. At 295 K, $D_m = 1{\cdot}45\ (8)$, $D_x = 1{\cdot}430$ g cm^{-3}, μ(Mo $K\alpha$) = 0·4587 cm^{-1}; at 163 K, $D_x = 1{\cdot}477$ g cm^{-3}. Anisotropic damage is suffered by exposure to Mo $K\alpha$ radiation both at 295 and 163 K; correction for this effect results in an internal agreement indicator R_{int} on F_m at 295 K of 0·0187 and, on F_m at 163 K, 0·0339. The Re atom undergoes such severe anharmonic oscillation at 295 K that P was the only other atom detectable in subsequent analysis without adequate thermal motion modelling. Inclusion of all tensor coefficients to seventh order in the Gram–Charlier expansion for the probability density function led to a final structural solution. Refinement on F_m^2 measured at 295 K by least squares gave the indicators (on F_m): $R = 0{\cdot}0132$, $wR = 0{\cdot}0119$ and $S = 0{\cdot}902$ for 2391 independent observations (averaged over the full form) with $F_m^2 \geq 3\sigma(F_m^2)$. The eight H atoms and one P atom form a distorted equatorially girdled trigonal prism about Re with the P atom occupying a prism corner. The average Re–H distance is 1·92 (11) Å and Re–P distance is 2·419 (3) Å; the systematic increase in both distances is a function of the Re-atom anharmonic motion. The cation is disordered at 295 K, with local pseudo-inversion through the N atom. The low-temperature phase contains two independent molecules in the asymmetric unit with coordinates related to those of the high-temperature phase by a simple transformation and displacement. The anionic displacements between the phases at 295 and 163 K do not exceed 0·25 Å, but atoms in the cation undergo displacements over this temperature interval as large as 1·8 Å. Refinement on F_m^2 at 163 K gave $R(F_m) = 0{\cdot}0645$, $wR = 0{\cdot}0638$, and $S = 2{\cdot}038$ for 6306 $F_m^2 \geq 3\sigma(F_m^2)$. Severe anharmonic motion by the two independent Re atoms remains present at 163 K and was fitted to sixth order in the Gram–Charlier expansion. The lower quality data at 163 K did not allow the H atoms to be located. The Re–P distances in the two independent anions at 163 K are 2·397 (10) and 2·422 (11) Å.

Introduction

The molecular structures of numerous transition-metal polyhydrides have been reported. The first determination of an Re polyhydride was that of K_2ReH_9 in which it was shown by neutron diffraction that the ReH_9^{2-} anion forms a regular equatorially tricapped

0108-7681/89/010052-09$03.00